Hydrodynamic behavior analysis of pulsed disc and doughnut column by CFD-PBM with modified drag law

Boren Tan[1], Dongbing Xu[1], Yong Wang[1], and tao qi[1]

[1]Institute of Process Engineering Chinese Academy of Sciences

June 18, 2020

Abstract

With increasing pulsation intensity from zero, the dispersed-phase holdup in pulsed disc and doughnut column (PDDC) decreases at first and then increases, which forms a U-shape trend. In this study, the modified drag law which is to account for the effect of turbulence is used for predicting the dispersed holdup with Computational Fluid Dynamics (CFD) simulations. The population balance model (PBM) kernel functions obtained from literatures are coupled with the CFD method to investigate the influence of drag law on the hydraulic performance of PDDC. The results indicate that the U-shape trend of dispersed holdup is successfully predicted with the modified drag law. The droplet size distribution and Sauter mean diameter with modified drag law is predicted better than that with Schiller-Nauman drag law. Local hydraulic performance and drag force field are illustrated to depict the typical flow behaviors in PDDC.

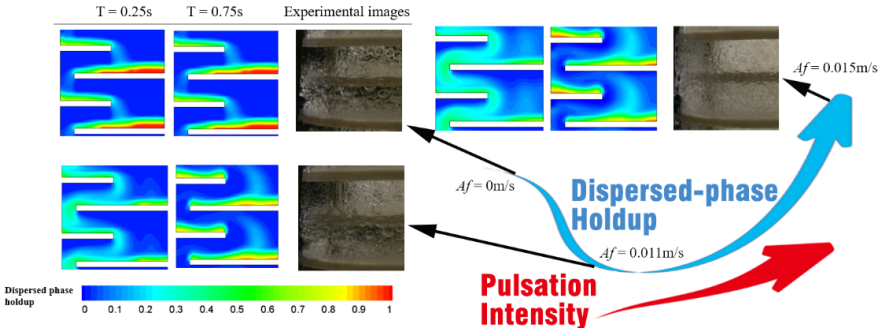

Hydrodynamic behavior analysis of pulsed disc and doughnut column by CFD-PBM with modified drag law

Boren Tan[a,b], Dongbing Xu[a], Yong Wang[a,c]11* To whom should be corresponded: wangyong@ipe.ac.cn and tqgreen@ipe.ac.cn, Tao Qi[a,d*]

[a] *Institute of process engineering, Chinese Academy of Sciences, Beijing, 100089, China.*

[b] *University of Chinese Academy of Sciences, Beijing, 101400, China.*

[c] *Innovation Academy for Green Manufacture, Chinese Academy of Sciences, Beijing, 100190, China*

[d] *Institute of Rare Earths, Chinese Academy of Sciences, Ganzhou, 341000, China*

ABSTRACT

With increasing pulsation intensity from zero, the dispersed-phase holdup in pulsed disc and doughnut column (PDDC) decreases at first and then increases, which forms a U-shape trend. In this study, the

modified drag law which is to account for the effect of turbulence is used for predicting the dispersed holdup with Computational Fluid Dynamics (CFD) simulations. The population balance model (PBM) kernel functions obtained from literatures are coupled with the CFD method to investigate the influence of drag law on the hydraulic performance of PDDC. The results indicate that the U-shape trend of dispersed holdup is successfully predicted with the modified drag law. The droplet size distribution and Sauter mean diameter with modified drag law is predicted better than that with Schiller-Nauman drag law. Local hydraulic performance and drag force field are illustrated to depict the typical flow behaviors in PDDC.

Keywords: Pulsed disc and doughnut column, Computational fluid dynamics, Population balance model, Drag model, Dispersed phase holdup

Introduction

Liquid-liquid extraction is one of classical methods used in separation process. Solvent extraction columns with disc and doughnut internals (disc and doughnut column, DDC) have been used for a range of applications in the chemical, petroleum, nuclear, hydrometallurgical industries and other areas for many years.[1] In the column, pulsing may be introduced by compressed air (pulsed disc and doughnut column, PDDC).

Knowledge of the hydrodynamic parameters including drop size and dispersed phase holdup (x_{d}) are important for design of liquid-liquid extraction columns as they are related to the interfacial area for mass transfer and the allowable throughputs.[2] Several experimental studies have been reported on PDDCs in the open literature.[3-5] With increasing pulsation intensity from zero, the dispersed-phase holdup decreases at first and then increases, which forms a U-shape trend.[3,6,7] Sauter mean diameter (d_{32}) decreases with an increase of pulsation intensity [2,8]. Hence, the interfacial area initially decreases before increasing result in a U-shape trend of overall mass transfer coefficient.[9,10] The possible mechanism of U-shape trend of dispersed holdup has been explained by the change of flow regimes[6], but there is still lack of validation through fluid simulation.

Recently, Computational fluid dynamics (CFD) has been emerged as a promising method to analyze phase flow phenomena.[11-13]Based on experimental work, some researchers conducted the two-phase CFD simulation on the pulsed columns by the Euler-Euler method with a global constant diameter.[14-17] Yi et al.[18]provided a thorough hydrodynamic description of pulsed sieve-plate column (PSPC) by CFD simulation and the predicted results was found underestimating the holdup in low-pulsation region. Saini et al.[19] investigated the variations of dispersed phase holdup with the operating condition and density ratios of the liquids in PDDC. The holdup of dispersed phase was reported to decrease linearly with the increase of pulsation intensity.

In order to capture the effect of collisions among drops on dispersed phase holdup in PDDC, Sarkar et al.[20] modified the momentum equation of the dispersed phase by introducing a collision model. The simulation of axial dispersion in PDDC was also carried out. Validation was done for varying operating conditions.[21] Considering the drag force acting on each particle is affected by the presence of surrounding particles, Retieb et al.[14] used the drag model of Wallis[22] to the CFD simulation of two-phase flow in PDDC. Sen et al.[23] also compared different drag models and the Kumar-Hartland drag model [24] were modified to better predict dispersed phase holdup.

Furthermore, Population balance model (PBM) implemented through CFD-PBM coupling method provides an opportunity to represent the liquid-liquid flow behaviors realistically. Using the kernel functions of Coulaloglou and Tavlarides[25], Amokrane et al.[26,27] conducted CFD-PBM simulation to predicted dispersed holdup and d_{32} in PDDC. Zhou et al.[28] proposed experimental correlations of droplet breakage kernel functions by directly measurement in PDDC and a CFD-PBM simulation was carried out to investigated local hydraulic performance.[29] In the CFD-PBM simulation of PSPC, Sen et al.[30] optimized Kumar-Hartland drag model[24] to reduce the error in dispersed phase holdup prediction.

However, it should be noted that U-shape trend of dispersed holdup in pulsed column has not been studied

in any of the above-mentioned studies. Drag force is the most important interphase force, which reduces the residence time of droplet leading to an increasing of dispersed holdup.[31,32] Simulating the U-shape trend of dispersed holdup can be helpful to understanding the interphase force, and improve the accuracy of CFD-PBM simulation as the coalescence functions are affected by the dispersed holdup.[33,34]

In present work, the U-shape trend of x_{d} was simulated using different drag coefficient models and the results are compared with our previous experimental data[2,3] The variation of drag force acting on the droplets are investigated and the drag law was modified. Then breakup and coalescence kernels obtained from literatures are improvement and coupled with the CFD method. Hydrodynamic performance including droplet size distribution, Sauter mean diameter and dispersed holdup are generated by the CFD-PBM method with the modified Schiller-Nauman drag law. Local hydraulic performances and local liquid-liquid flow behaviors are also discussed with simulation results.

CFD-PBM model

Euler-Euler and Turbulence model

The two-phase flow in this study is described by the Eulerian-Eulerian model which mathematically treats the two phases as interpenetrating continua. The aqueous phase is set as the dispersed phase (second phase), d , while the organic phase is the continuous phase (primary phase), c . The conservation equations solved for each phase are shown as follows:

Continuity equation for phase i :

$$\frac{\partial\left(\alpha_i \rho_i\right)}{\partial t}+\nabla\left(\alpha_i \rho_i u_i\right)=0 \tag{1}$$

Momentum conservation equation for phase i :

$$\frac{\partial\left(\alpha_i \rho_i u_i\right)}{\partial t}+\nabla\left(\alpha_i \rho_i u_i u_i\right)-\nabla \tau_i=$$

$$-\alpha_i \nabla p+\alpha_i \rho_i \mathrm{g}+\left(F_i+F_{i,lift}+F_{i,vm}\right) \tag{2}$$

In the equations above, α represents the volume fraction,ρ represents density, u is phase velocity,τ is the stress-strain tensor, p is the pressure shared by all phases, g is gravitational acceleration,F_i is the external body force,$F_{i,lift}$ is the lift force,$F_{i,vm}$ the virtual mass force acting on the$i$ th phase. R_{ij} is the interaction force between i th and j th phase. The subscript $i$represents phase i . Because here we only consider the two-phase condition, volume fractions of the two phases at every mesh unit should satisfy:

$$\alpha_c+\alpha_d=1 \tag{3}$$

In most cases, the lift force and virtual mass force are insignificant compared to the drag force and are thus often neglected in two-phase CFD simulations of liquid-liquid dispersed flows. [15,35,36]The drag force term between the continuous and dispersed phase is defined in terms of the interphase exchange coefficient ($F_{c,d}$) as:

$$\sum R_{c,d}=\sum F_{c,d}\left(u_c-u_d\right) \tag{4}$$

where the interphase exchange coefficient is calculated as:

$$F_{c,d} = \frac{\rho_d \alpha_c \alpha_d f}{\tau_d} \tag{5}$$

Where f represents the drag function and τ_d is the particulate relaxation time, which is defined as:

$$\tau_d = \frac{\rho_d d_{32}^2}{18\mu_c} \tag{6}$$

where μ is dynamic viscosity. d_{32} is the Sauter mean diameter of the dispersed phase which is calculated from the following equation:

$$d_{32} = \frac{\sum_{i=1}^{n} n_i d_i^3}{\sum_{i=1}^{n} n_i d_i^2} \tag{7}$$

where n_i is number of droplets.

The definitions of f include a drag coefficient (C_D) that is based on the relative Reynolds number (Re). In liquid-liquid system, the drag function is defined as:

$$f = \frac{C_D \mathrm{Re}}{24} \tag{8}$$

in which the relative Reynolds number is defined as:

$$Re = \frac{\rho_c V_r d_{32}}{\mu_c} \tag{9}$$

where V_r represents apparent relative velocity between the continuous and dispersed phase.

By combining the above equations, the drag force term can be represented as follows:

$$R_{c,d} = \frac{3\rho_d \alpha_c \alpha_d C_D V_r \left(u_c - u_d\right)}{4 d_{32}} \tag{10}$$

The realizable k -ϵ mixture turbulence model is used to describe multiphase turbulence, which is extended from the single-phase version. This model consists of partial differential equations for turbulence kinetic energy k and its dissipation rate ϵ .

$$\frac{\partial}{\partial t}\left(\rho_m k\right) + \nabla \bullet \left(\rho_l u_m k\right) = \nabla \bullet \left(\frac{\mu_{t,m}}{\sigma_k} \nabla k\right) + G_{k,m} + G_{b,m} - \rho_m \varepsilon \tag{11}$$

$$\frac{\partial}{\partial t}\left(\rho_m \varepsilon\right) + \nabla \bullet \left(\rho_l u_m \varepsilon\right) = \nabla \bullet \left(\frac{\mu_{t,m}}{\sigma_\varepsilon} \nabla \varepsilon\right) + \rho_m C_1 \Sigma \mathrm{\varepsilon}$$

$$-\rho_m C_2 \tfrac{\varepsilon}{k+\sqrt{\mathrm{\varepsilon}}} + C_{1\varepsilon} \tfrac{\varepsilon}{k} C_{3\varepsilon} G_b \tag{12}$$

$$C_1 = max\left(0.43, \frac{\eta}{\eta + 5}\right), \eta = S\frac{k}{\varepsilon} \tag{13}$$

Where S represents the strain rate tensor. G_{k} represents the generation of turbulence kinetic energy due to the mean velocity gradients and G_{b} is the generation of turbulence kinetic energy due to buoyancy. The subscript m refers to the mixture of the two phases. The mixture averaged values of the density and velocity are defined as:

$$\rho_m = \alpha_c \rho_c + \alpha_d \rho_d \tag{14}$$

$$u_m = \frac{\alpha_c \rho_c u_c + \alpha_d \rho_d u_d}{\alpha_c \rho_c + \alpha_d \rho_d} \tag{15}$$

$$\mu_{t,m} = \rho_m C_\mu \frac{k^2}{\varepsilon} \tag{16}$$

Drumm et al.[11] compared different turbulence models' results with PIV experiment data and suggested realizable$k$ -ϵ model is the sufficient to describe two phase behavior. Therefore, this model has been used in this study with the default values for C_{1}, $C_{2}$and σ_{μ} .

Drag coefficient model

The drag coefficient in Eq. (8) is used as a local model of the stationary drag term to be implemented into CFD two-phase codes. It is this drag coefficient model that differs among the exchange-coefficient models. The drag coefficient correlations for a single sphere has been thoroughly studied. The model (Eq. 17) proposed by Schiller and Nauman[37] is seems to be the most reliable for drops considered as rigid spheres and has been experimentally checked by Bardin-Monnier[38].

In a multiparticle system, the drag force acting on each particle is affected by the presence of surrounding particles. A number of empirical correlations have been derived to account for this effect.[39] These models have been reported in Table 1.

Ishii and Zuber [40] proposed a drag law for particulate flows (Eq. 18), gas-liquid and liquid-liquid systems, including the case of distorted inclusions. They also reached a satisfied prediction of experimental slip velocity in a wide range of flow parameters. Kumar and Hartland[24] proposed an empirical drag law (Eq. 19) for liquid-liquid systems based on a large number of experimental data with nearly 30 different liquid-liquid systems, which covered an wide range of particle Reynolds, Eotvos numbers and dispersed phase fraction.

Retieb et al.[14] compared the influence of dispersed phase holdup, x_{d}, on the drag coefficient. For holdup values x_{d}<20%, there is quite good agreement between all correlations. The model of Wallis[22] was successfully applied to the study of two-phase turbulent countercurrent flows in PDDC. Sen et al.[23] also evaluated the suitability of different drag models for predicting dispersed phase holdup. Kumar-Hartland drag model was found to be the best among the reported drag models and the parameters were modified to better predict the holdup.

Table 1. Drag Coefficient Models

References	Models
Schiller and Nauman (1935) [37]	$C_D = \begin{cases} \frac{24}{\mathrm{Re}}\left(1 + 0.15\mathrm{Re}^{0.687}\right) & Re \leq 1000 \\ 0.44 & Re > 1000 \end{cases}$

References	Models
Ishii and Zuber (1979) [40]	$C_D = \frac{24}{\mathrm{Re}_m}\left(1+0.1\mathrm{Re}_m^{0.75}\right);$ $\mathrm{Re}_m = \frac{\rho_c d_d \lvert u_d - u_c\rvert}{\mu_m}; \mu_m = \mu_c\left(1-\frac{x_d}{x_{d,m}}\right)^{-2.5 x_{d,m}\frac{\mu_d+0.4\mu_c}{\mu_d+\mu_c}}$
Wallis (1974) [22]	$C_D = \frac{24}{\mathrm{Re}}\left(1+0.15\mathrm{Re}^{0.687}\right)(1-x_d)^{-4.7}$ (19)
Kumar and Hartland (1985) [24]	$C_D = \left(0.53+\frac{24}{Re}\right)\left(1+4.56{x_d}^{0.73}\right)$ (20)
Sen et al. (2016)[23]	$C_D = \begin{cases}\left(0.53+\frac{24}{\mathrm{Re}}\right)\left(1+6.2{x_d}^{0.4}\right) & for \quad Af < 0.025 m/s \\ \left(0.53+\frac{24}{\mathrm{Re}}\right)\left(1+10.0{x_d}^{0.4}\right) & for \quad Af \geq 0.025 m/s\end{cases}$ (21)

A working solution can be achieved by lumping all uncertainty in one or two terms of the governing equations and modifying these terms to bring the predicted results closer to the experimental results. In Euler-Euler model of dispersed two-phase flow, drag model is the term often modified to bring predictions closer to the measured values.[23,41,42] In this study, different drag models listed in Table 1 are used to evaluate the CFD simulation of two-phase flow.

Population balance model

The PBM describes number density of droplets with specific size over space and time, and the population balance equation (PBE), which is a general form of the number density function, can be written as:

$$\frac{\partial n(d;\ x,\ t)}{\partial t} + u \bullet \nabla n\left(d;\ x,\ t\right) - \nabla \bullet \left(\Gamma_t \nabla n\left(d;\ x,\ t\right)\right) = S\left(d,\ t\right) \tag{22}$$

Where x is the coordinates in physical space, $t$is the time coordinate and d denotes the drop diameter.$n\left(d; x,\ t\right)$ is the number density function of the droplets and thus$n\left(d; x,\ t\right)\mathrm{d}d$ represents the number of droplets with size range from d to d +d(d) per unit volume. u is the velocity in physical space andΓ_t is the effective diffusion coefficient of the number density. The source term $S\left(d,\ t\right)$, which takes into account the influence of breakage and coalescence processes, includes four parts as follows:

$$S\left(d,\ t\right) = B^C\left(d,\ t\right) - D^C\left(d,t\right) + B^B\left(d,\ t\right) - D^B\left(d,t\right) \tag{23}$$

Where $B^C\left(d,\ t\right)$ and$B^B\left(d,\ t\right)$ represent the birth rates of drops with diameter d at any time t due to coalescence and breakage, respectively. $D^C\left(d,t\right)$ and$D^B\left(d,t\right)$ represent the death rates of drops with diameter d at any time t due to coalescence and breakage, respectively. When only binary breakup and coalescence are considered, the expressions of the birth and death rate are given by Eqs. (24-27).

$$B^C\left(d,t\right) = \frac{1}{2}\int_0^d n\left(\sqrt[3]{d^3-d'^3},\ t\right) n\left(d',\ t\right) a\left(\sqrt[3]{d^3-d'^3},\ d'\right)$$

$$\times \frac{d^2}{\sqrt[3]{\left(d^3 - d'^3\right)^2}} dd' \tag{24}$$

$$B^B\left(d,\ t\right) = \int_0^\infty \beta\left(d, d'\right) \mathrm{g}(d') n\left(d', t\right) dd' \tag{25}$$

$$D^C\left(d,\ t\right) = n\left(d, t\right) \int_0^\infty n\left(d', t\right) a\left(d, d'\right) dd' \tag{26}$$

$$D^B\left(d,\ t\right) = \mathrm{g}\left(d\right) n\left(d, t\right) \tag{27}$$

Where g(d) is the breakup frequency function and $\beta\left(d, d'\right)$ is the daughter size distribution function. Thus, $\beta\left(d, d'\right)$ ddrepresents the probability to generate droplet of size from d to$d$ +d(d) when a mother droplet of size d' is broken-up. a$\left(d,\ d'\right)$ is the coalescence frequency function which represents the probability of successful collisions between droplets of size d and d'. It is defined as the product of the collision frequency h and the coalescence efficiency λ.

$$a\left(d, d'\right) = h\left(d, d'\right) \bullet \lambda\left(d, d'\right) \tag{28}$$

In literature, several kernels have been derived theoretically. Precise kernel functions must be determined before a CFD-PBM simulation to be performed. The PBM kernel functions derived by Coulaloglou and Tavlarides[25] have been widely used by numerous researchers.

$$\mathrm{g}\left(d\right) = C_1 \frac{\varepsilon^{1/3}}{d^{2/3}(1 + x_d)} \exp\left(-\frac{C_2 \gamma (1 + x_d)^2}{\rho_d \varepsilon^{2/3} d^{5/3}}\right) \tag{29}$$

$$\beta\left(d, d'\right) = 7.2 \frac{d^2}{d_m^3} \exp\left(-4.5 \frac{\left(2d^3 - d'^3\right)^2}{d'^6}\right) \tag{30}$$

$$h\left(d, d'\right) = C_3 \frac{\varepsilon^{1/3}}{(1 + x_d)} \left(d + d'\right)^2 \left(d^{2/3} + d'^{2/3}\right)^{1/2} \tag{31}$$

$$\lambda\left(d, d'\right) = \exp\left(-C_4 \frac{\mu_c \rho_c \varepsilon}{\gamma^2 \left(1 + x_d\right)^3} \left(\frac{dd'}{d + d'}\right)^4\right) \tag{32}$$

Amokrane et al.[27] adjusted the parameters of those kernels by fitting the models' parameters to the measured droplets size distribution (DSD) in PDDC. CFD-PBM simulations were carried out with the modified kernels. Considering the lack of suitable PBM kernel functions in the PDDC, experimental correlations of droplet breakage kernel functions were proposed by Zhou et al.[28]

$$\mathrm{g}\left(d\right) = Z_1 \frac{\left(\varepsilon \bullet 1m\right)^{1/3}}{h} \left(\left(\varepsilon \bullet 1m\right)^{1/3} \left(\frac{\rho_c}{\gamma \mathrm{g}}\right)^{0.25}\right)^{Z_2} \left(\left(\varepsilon \bullet 1m\right)^{1/3} \frac{\rho_c}{\mu_d} d\right)^{Z_3} \tag{33}$$

$$\beta\left(d\middle|d^{'}\right)=\begin{cases}14.55\frac{d^2}{d^{'3}}\left(\frac{d^3}{d^{'3}}\right)^{0.59}\left(d^{'}\left(\frac{\rho_c g}{\gamma}\right)^{0.5}\right)^{-0.049}, & \frac{d^3}{d^{'3}}\leq 0.5\ and\ d^{'}>d_c\\ 2.88\frac{d^2}{d^{'3}}\left(\frac{d^3}{d^{'3}}\right)^{-0.4}\left(d^{'}\left(\frac{\rho_c g}{\gamma}\right)^{0.5}\right)^{0.17}, & \frac{d^3}{d^{'3}}\leq 0.5\ and\ d^{'}\leq d_c\end{cases} \tag{34}$$

$$d_c=1276.5\frac{\mu_d}{(\varepsilon\bullet 1m)^{1/3}\rho_c}\left((\varepsilon\bullet 1m)^{1/3}\left(\frac{\rho_c}{\gamma g}\right)^{0.25}\right)^{-0.89} \tag{35}$$

The DSD results under several operation conditions simulated with the two different breakup functions are compared. The results show that Coulaloglou and Tavlarides model[25] underestimates the droplet breakage frequency, especially for large droplets. The results calculated by the model of Zhou et al.[28] exhibits better agreements with experimental.[29] Hence, the breakage, daughter droplet distribution kernels of Zhou et al.[28] (Eqs 33-35) and coalescence kernels of Coulaloglou and Tavlarides[25] (Eqs 31-32) are used in this study.

Numerical procedure

For validation, the experimental data on dispersed phase holdup and drop diameter reported in a previous study are used.[2,3] The general column arrangement is shown in Fig. 1 (a) and the key dimensions of the pilot plant column are shown in Table 2. The organic phase (continuous phase) used in this study is 3 vol % Alamine 336 (tri-n-octylamine) and 1 vol % isodecanol in Shellsoll 2046. The aqueous phase (dispersed phase) used is tap water. The physical properties of the experimental system used in this study are shown in Table 3.

Table 2 Geometry parameters of PDDC.

Parameters	Dimensions
Column diameter, D	72.5 mm
Effective column height, H	815 mm
Compartment height, h_c	19 mm
Dis diameter, D_c	42.6 mm
Doughnut aperture, D_a	36.9 mm
Free area, e	25.9%

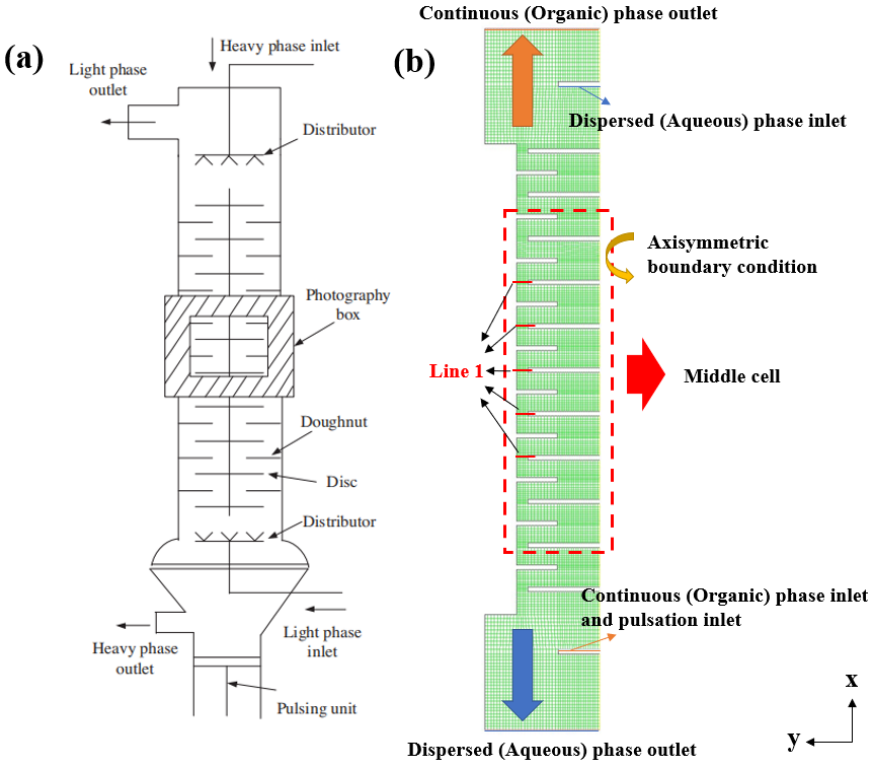

Fig. 1 Calculation domain of PDDC. (a) Schematic diagrams of PDDC; (b) mesh for calculation domain.

Table 3. Physical properties of the aqueous and organic phases (25)

	Aqueous	Organic
Density (kg/m^3)	998	805
Viscosity (Pa[?]s)	1×10^{-3}	1.85×10^{-3}
Interfacial tension (N/m)	0.011	0.011

The single-phase flow simulation results indicate that the flow field in the PDDC is symmetric and 2D simplification of the pulsed-flow modelling is fully justified.[43] A 2D axis-symmetric grid is used as a result of the rotational symmetry of a disc and doughnut column. Adequacy of limited number of column internals to reduce computational time is reported in pulsed columns.[11,14,36] The calculation domain is depicted in Fig. 1(b). The mesh is constructed with quadrilateral grids and the mesh size is set to be 1 mm.

The coupling of PBM with the CFD is based on the Euler-Euler framework. According to Yu et al.,[29] using a universal droplet size range for all operation conditions is not advisable. A reasonable droplet size range for every operation condition is estimated according to experimental results. 10 bins are used to represent the range of drop diameter. The simulation conditions and discretization parameters are listed in Table 4. The smaller drops are sufficiently captured due to non-linear bin size used. The exponent, q , is used in the discretization of the growth term diameter coordinate:

$$\frac{d_{i+1}}{d_i} = 2^{q/3}, \qquad where \;\; i = 0,\; 1,\; \ldots 9 \tag{36}$$

Table 4. Determination of droplet size under different operation conditions.

Operation Conditions	1	2	3	4	5
Pulsation Intensity Af (m/s)	0	0.0067	0.0111	0.0132	0.0153
Dispersed phase velocity V_{d} ($\times 10^{-3}$m/s)	0.808˜2.50	0.808˜2.50	0.808˜2.50	0.808˜2.50	0.808˜2.50
Minimum droplet diameter (mm)	1.5	1.0	0.5	0.5	0.5
Exponent q	0.7	0.8	0.95	0.8	0.7
Drop size range (mm)	[1.5, 6.4]	[1.0, 5.2]	[0.5, 3.6]	[0.5, 2.6]	[0.5, 2.1]

The boundary conditions are properly set as shown in Fig. 1(b). The side of plane is set to an axisymmetric condition. One pressure outlet condition is used at the top boundary for organic outlet, while three velocity inlet conditions are used for the aqueous inlet, aqueous outlet, and organic inlet boundaries. The inlet of organic phase is superposed on the pulsation input and the velocity at the boundary is expressed as:

$$u_{\mathrm{cm}} = u_c + u_p = u_c + \pi A f \left(\frac{D}{D_{\mathrm{cm}}}\right)^2 \sin\left(2\pi f t\right) \tag{37}$$

where D is the column diameter and D_{cm} is the diameter of the organic inlet where pulsatile velocity boundary condition is applied.

In the CFD simulation with a global constant diameter, Sauter mean diameter of the dispersed phase is set according to experimental data. In the CFD-PBM simulation, droplets with a maximum diameter exist at the inlet. All internal walls are set with a no-slip condition, and the near-wall region is modelled with standard wall function.

Simulations are carried out using commercial CFD software *Fluent student 2019R2* . Transient-state simulation is with a time step of 0.002s, while the second-order implicit solver is used. The realizable$k$ -ϵ turbulent model is used for the closure of the Reynolds-averaged Naiver-Stokes equations. Convergence of the solution is considered when the residual of the equations is less than 10^{-4}.

Results and discussion

Comparison of different drag models

The dispersed phase holdup, x_{d}, is defined as the volume fraction of the active section of the column that is occupied by the dispersed phase

$$x_d = \frac{v_d}{v_d + v_c} \tag{38}$$

In pulsed column holdup decreases first and then increases with an increase of pulsation intensity, which forms a U-shape trend.[44,45] The effects of pulsation intensity, Af , on holdup for PDDC are investigated with CFD, and the results are compared with the experimental data reported by in our previous work.[3] Table 5 lists the conditions for each simulation. Pulsation intensity varies from 0 to 0.0153 m/s. Holdup values predicted by using different drag coefficient models in two-phase CFD simulations are also shown in Fig. 2. The flow fields and variables change periodically in the PDDC due to the sinusoidal pulsation. The time-average over a periodic cycle and surface-average in the middle cell are required to obtain simulation results.

It can be seen from Fig. 2 that the CFD model with all current drag models fails to predict the dispersed phase holdup at the high pulsation intensity, which is in agreement with the CFD model outcomes presented by Sen et al. [30] with a pulsed sieve plate column. In order to explain this performance, simulated drag force with different conditions are investigated.

Table 5 Conditions and data used for simulations

Trial	Af (m/s)	x_{d}	d_{32} (mm)
1	0	9.66%	3.72
2	0.0067	4.76%	2.72
3	0.0111	4.43%	2.03
4	0.0132	5.20%	1.47
5	0.0153	5.65%	1.31

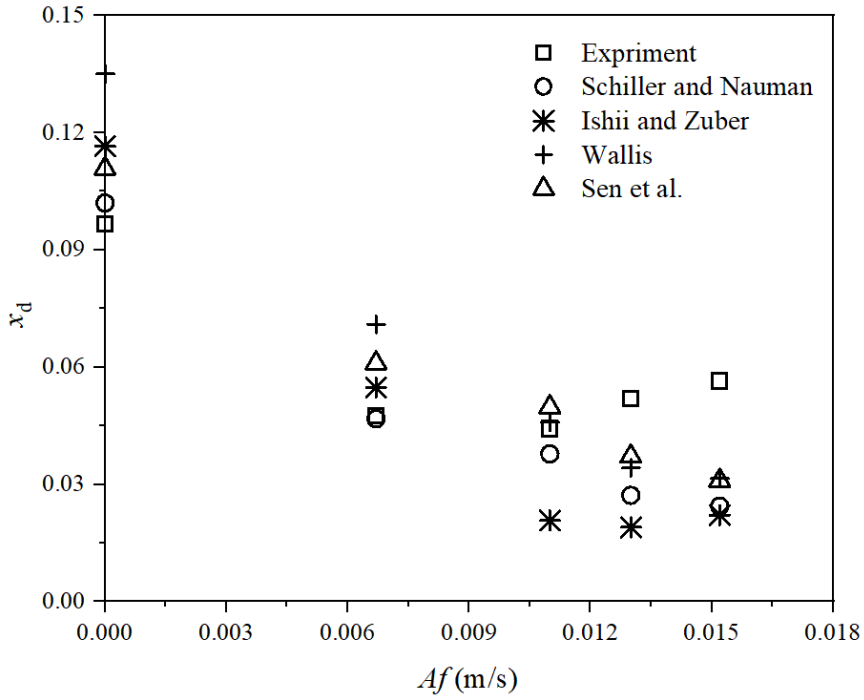

Fig. 2 Comparison between experimental and CFD simulation results of holdup under various pulsation intensities (V_{c}=6.25×10^{-4} m/s, V_{d} = 8.08×10^{-4} m/s)

As 2D axis-symmetric grid is used for the simulation of PDDC, vectors have no tangential component. The apparent relative velocity, V_r, in Eq. (9) is calculated by Eq. (39).

$$V_r = |u_c - u_d| = \sqrt{{V_x}^2 + {V_y}^2} \tag{39}$$

where V_x and V_y represent the relative axial and radial velocities, which can be calculated from:

$$V_x = |V_{c,x} - V_{d,x}| \tag{40}$$

$$V_y = |V_{c,y} - V_{d,y}| \tag{41}$$

Where $V_{c,x}$ and $V_{c,y}$ represents the axial and radial velocities of continuous phase. $V_{d,x}$ and $V_{d,y}$ represents the axial and radial velocities of dispersed phase. As the drag force is mainly from gap of internal, which prevent passage of dispersed phase.[46], the simulated results of V_x andV_y using different drag force coefficient models are analyzed in the gap between disc and wall of column (Line 1 in Fig.1 (b)). The results are shown

in Fig. 3, in which the value of V_x andV_y are obtained by time-averaged and surface-average over one pulsing cycle.

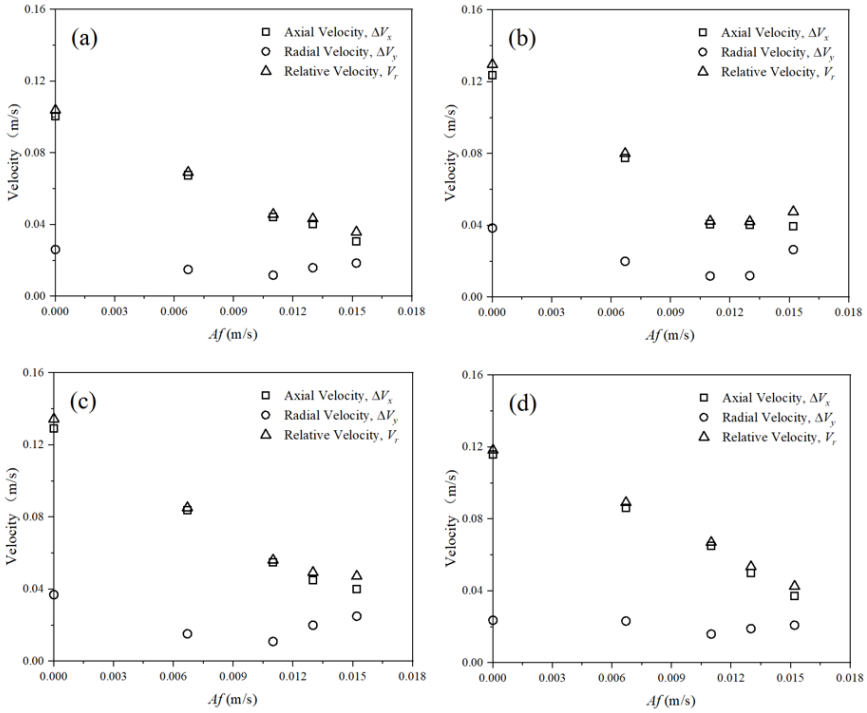

Fig. 3 Variation of relative velocity as function of pulsation intensity at the gap between disc and wall of column. (a) Schiller and Nauman model; (b) Ishii and Zuber model; (c) Wallis model; (d) Sen et al. model.

It can be seen in Fig.3 that the apparent relative velocity, V_{r}, decreases with the increase of pulsation intensity, and V_y is insignificant compared to V_x in low pulsation intensity (Af <0.01m/s). According to the quantitative analyses of apparent relative velocity, the drag coefficient and drag force term are then calculated by Eqs. 4-10 and shown in Fig. 4. It can be seen that the drag coefficient increased with the increase of pulsation intensity while the variation of drag force term is opposite. This is primarily due to the decrease of apparent relative velocity shown in Fig. 3 and the decrease of holdup in Fig. 2 can be attributed to decrease of drag force term.

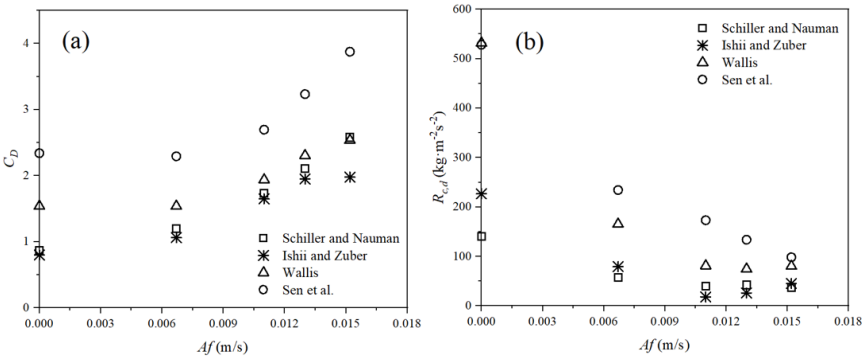

Fig. 4 Variation of drag force parameters as function of pulsation intensity. (a) drag coefficient, C_{D}; (b)

drag force term, $R_{c,d}$.

Drag law modification

The basic drag correlation is based on droplets moving in a still liquid and does not suitable the condition of droplets moving in turbulent liquid[47].

In this work, a modified drag law that takes into account the effect of turbulence is proposed. It is based on a modified viscosity term in the relative Reynolds number [48]:

$$Re = \frac{\rho_c V_r d_{32}}{\mu_c + C\mu_{t,m}} \tag{42}$$

where C is an empirical constant and $\mu_{t,m}$ is the turbulent viscosity which is calculated from Eq. (16). This method is inspired by the work of Barnea and Mizrahi[49], which used the modified viscosity approach to correct for mutual hindrance effects in bubble clouds. The value for C in Eq. (42) is an engineering estimate, which is suggested to 0.3 to 0.5[41,42,47].

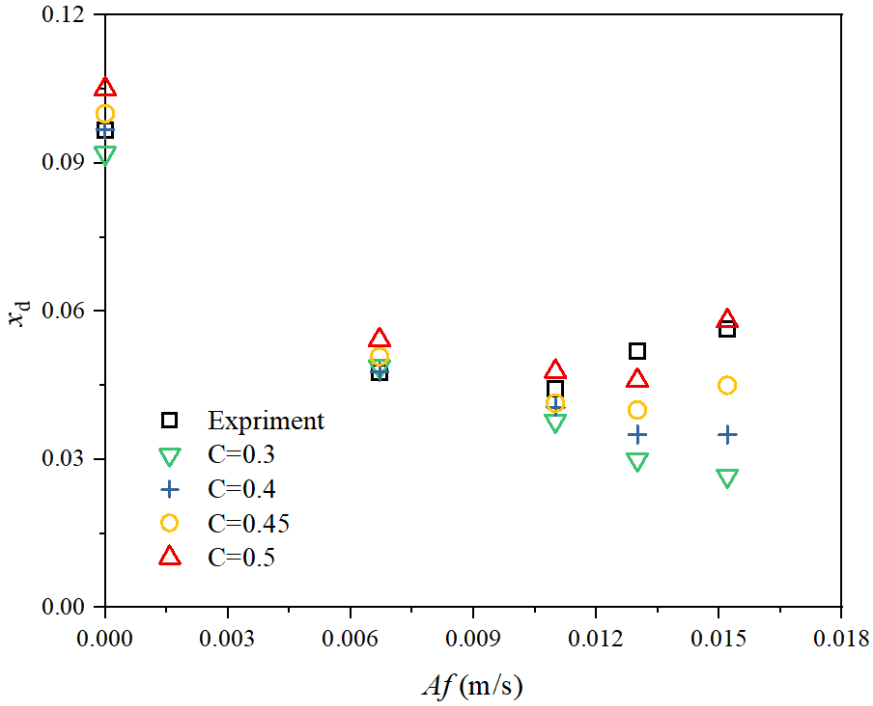

Fig. 5 Effect of parameters C on CFD simulated dispersed phase holdup

In order to determine suitable value of C , CFD simulations are carried out based on Schiller and Nauman model[37] (Fig. 5). It can be seen that, with the increase of C , prediction of holdup increases at the higher pulsation intensity and CFD model still predicts the same trend of decreasing holdup as before.

The deviation of simulated holdup from experimental data is measured with average relative deviation (AARD), defined as:

$$AARD\% = \frac{1}{n}\sum_{1}^{n}\frac{|\text{predicted value} - \text{experimental value}|}{\text{experimental value}} \times 100$$

where n is the number of data points. C =0.5 is found to predict the U-shape trend of holdup of PDDC well within 8.97% AARD.

CFD-PBM simulation

Table 4 lists the droplet size ranges for which conditions are used to simulate. As initial drop size distribution has no remarkable influence on steady simulation results, 100% maximum droplets is used as initial drop size distribution.

With the original values of parameters in the kernel functions, a relatively large deviation is observed between the predicted and experimental data for high pulsation intensity (Supplementary Material Fig. S1). An adjustment of the model parameters is therefore required. The following simplified procedure is implemented in Supplementary Material Fig. S2, which has been successfully used in an agitated-pulsed column.[50] The kernels with the adjusted values are listed in Table 6.

Table 6 Adjusted parameters in the kernels

C_3	C_4	Z_1	Z_2	Z_3
0.013	8.54×10^{9}	4.69×10^{-17}	0.35	4.8

3.3.1 Validation and comparison

The simulation cumulative volume droplet size distributions obtained with the modified drag law and Schiller-Nauman (S-N) drag law[37] are compared with the experimental reported in our previous study.[2] It can be seen from Fig. 6 that an acceptable agreement in the DSD is obtained between CFD-PBM simulation and experimental data, which indicate that the regressed parameters in Zhou's and Coulaloglou and Tavlarides' kernel functions can be successfully applied to the prediction of DSD in PDDC.

Compared with the modified drag law, S-N drag law tends to overestimate DSD under higher pulsation intensity. This is because the simulated holdup using S-N drag law is lower than experimental data, which reduces the coalescence frequency of droplets and hence the DSD moves toward left. However, Fig. 6 also indicates that the calculated proportion of small-size droplets is higher than the experimental results. The possible explanation is that Zhou's model predicts a high distribution probability with small-size droplets.

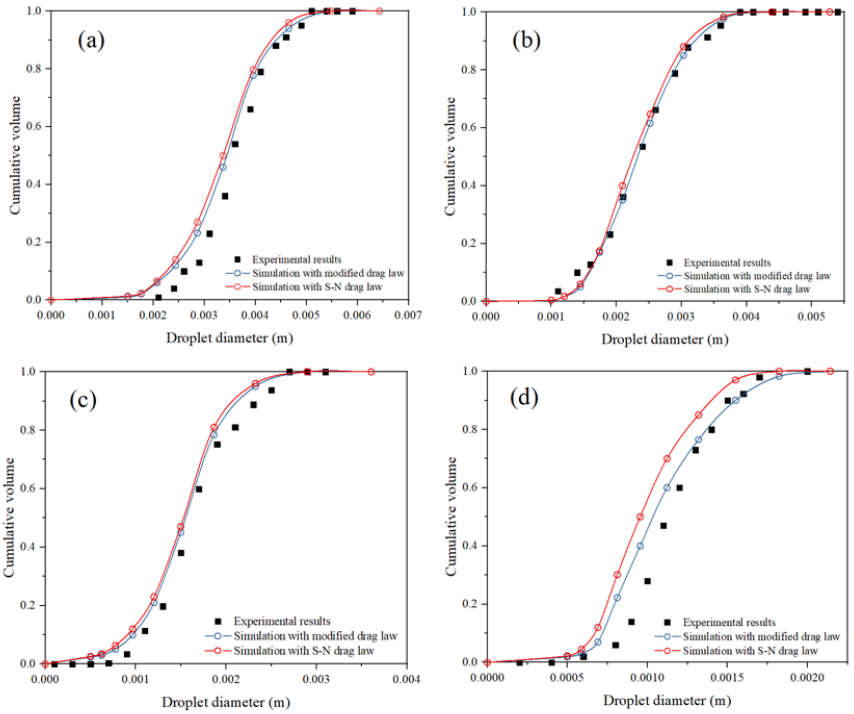

Fig. 6 Comparison between experimental and CFD-PBM simulation results on cumulative volume droplet size distribution, under various pulsation intensities (V_c =6.25×10^{-4}m/s, V_d = 8.08×10^{-4} m/s). (a)Af =0 m/s; (b) Af =0.0067 m/s; (c) Af =0.0111 m/s; (d)Af =0.0153 m/s.

Furthermore, the hydrodynamic parameters of dispersed phase holdup and Sauter mean drop diameter, d_{32}, are calculated by the droplet size distribution. Fig. 7 shows comparison of the predicted and experimental results on variation of dispersed phase holdup with pulsation intensity and dispersed phase velocity.

Compared with the numerical approaches with S-N drag law, the PBM-CFD simulations with the modified drag law can successfully predict the dispersed holdup under different pulsation intensity (Fig. 7(a)) and dispersed phase velocity (Fig. 7(b)). The AARD of holdup is 23.8% for the S-N drag law and 7.11% for the modified drag law.

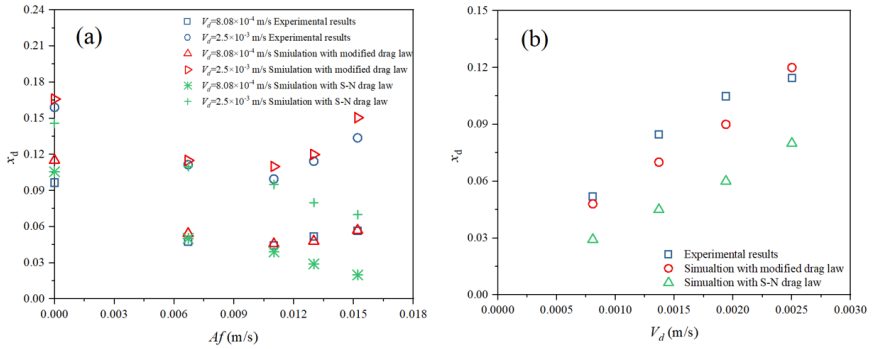

Fig. 7 Comparison between experimental and CFD-PBM simulation results of dispersed phase holdup. (a) V_c=6.25×10^{-4} m/s; (b) V_c=6.25×10^{-4} m/s, Af =0.0067 m/s.

The comparison of the predicted and experimental results on variation of d_{32} with pulsation intensity and dispersed phase velocity is shown in Fig.8. It can be seen that the d_{32} that calculated by the PBM-CFD with the modified drag law decreases with increase of pulsation intensity and slightly increases with increase continuous phase velocity, which agrees with experimental results well. The AARD of d_{32} is 9.8% for the S-N drag law and 6.3% for the modified drag law, which means the simulation results of d_{32} with modified drag law fit better with experimental data than S-N drag law.

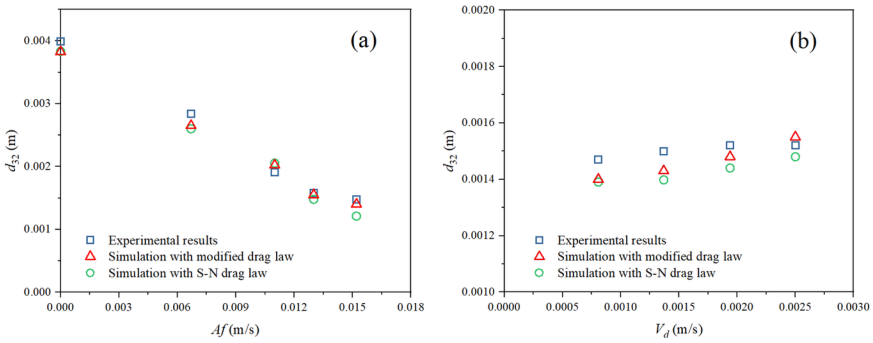

Fig. 8 Comparison between experimental and CFD-PBM simulation results of Sauter mean diameter, d_{32}, under various operated conditions. (a) V_c =6.25×10^{-4}m/s, V_d = 8.08×10^{-4} m/s; (b) V_c =6.25×10^{-4} m/s,Af =0.0067 m/s.

3.3.2 Local behaviors of two-phase flow

The CFD-PBM model is used to have detailed insights into the operation characteristics of the PDDC. Fig. 11 shows profiles of dispersed phase holdup predicted from the CFD-PBM simulations and experimental images under 3 different pulsation intensity. The experimental image for no-pulsation intensity condition (Af = 0m/s) shows that accumulation of the dispersed phase on the plates and the similar accumulation can also be observed in the CFD-PBM simulation. When pulsation is introduced into the system (Af = 0.011m/s), the dispersed phase is driven from the plates at the negative apex moment of the sinusoidal pulsation period (t = 0.25s) and tends to stay on the plates at the positive apex moment (t = 0.75s). With further increase in pulse velocity (Af = 0.015m/s), the experimental image shows more uniform distribution of dispersed phase, which can also be observed in CFD-PBM simulation.

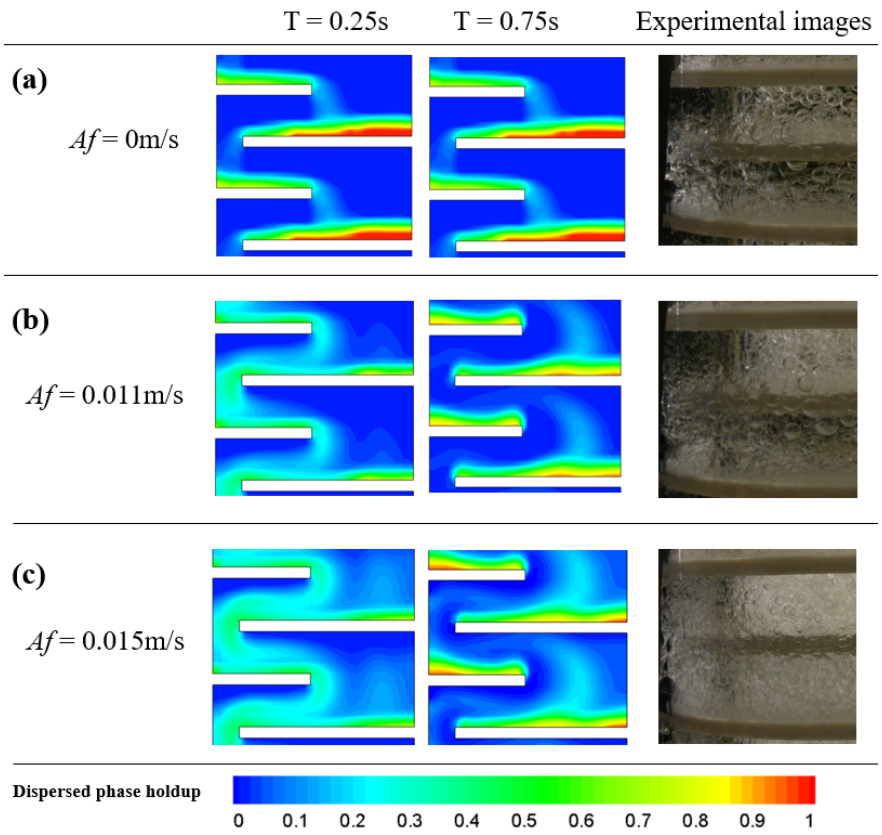

Fig. 9 Profile of dispersed holdup variations as obtained from CFD-PBM simulations and corresponding experimental images (V_c =6.25×10^{-4} m/s, V_d = 2.5×10^{-3} m/s)

Fig. 10 shows the distribution of Sauter mean diameter for two different values of pulsation intensity. A significant reduction in Sauter mean drop diameter could be observed as Af is increased from 0.011 to 0.0153 m/s, which indicates the drop size distribution become uniform. Large size droplets are introduced continuously from the dispersed phase inlet, which makes the mean droplet diameter at the top part larger than that at the lower part.[29,30] Generally, the minimum mean diameter is found at the edges of plate. This is attributed to the high turbulent energy dissipation rate at these locations, leading to a high breakup of droplets, and hence reduce the mean diameter.[29]

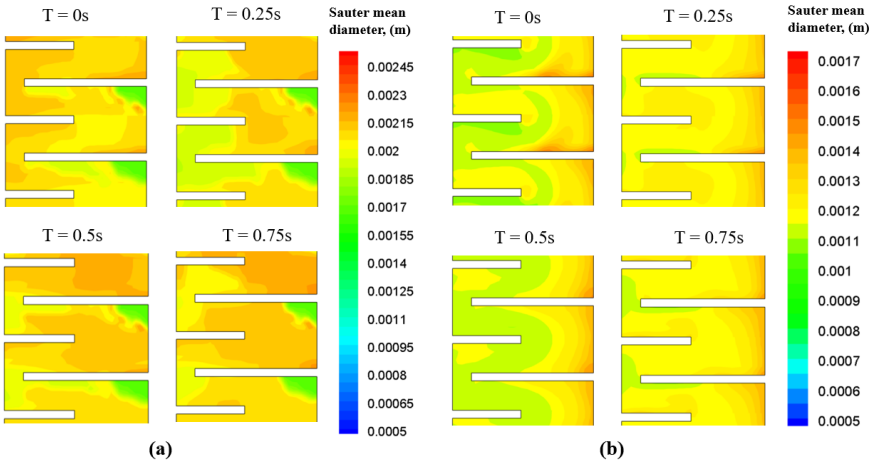

Fig. 10 Profile of Sauter mean diameter at four different moments selected during a pulsing period (V_c=6.25×10^{-4} m/s, V_d = 2.5×10^{-3} m/s). (a) Af = 0.0111 m/s; (b)Af = 0.0153 m/s.

The local relative velocity in a computational cell is also important as it influences the local drag force. Fig. 11 (a) describes the relative velocity during one pulsation cycle. The intensive velocity gradient is observed at negative (t = 0.25 s) and positive negative (t = 0.75s) peaks of the pulsing cycle. The maximum relative velocity is always found at the wall of plates, which leads to an exactly inverse situation for drag force coefficient as shown in Fig. 11 (b). This is due to higher values of apparent relative velocity which causes lower Reynold number leading to reduce of drag force coefficient.

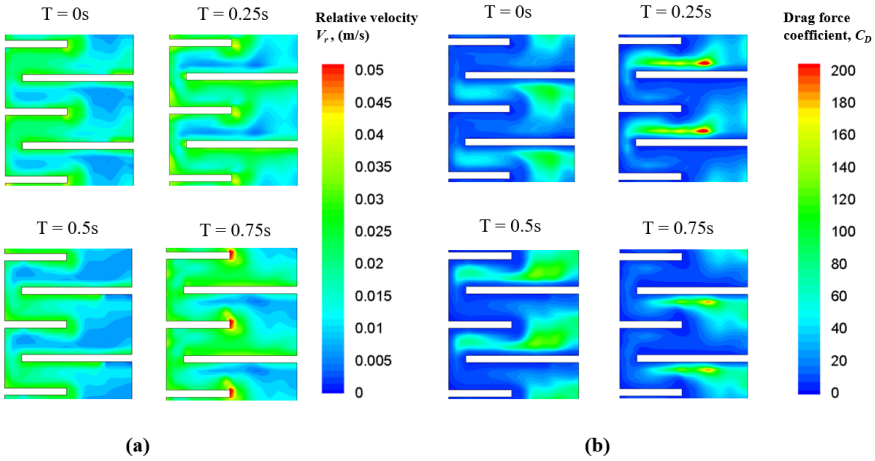

Fig. 11 Profile of apparent relative velocity and drag force coefficient at four different moments selected during a pulsing period (Af =0.0153 m/s, V_c=6.25×10^{-4} m/s, V_d = 2.5×10^{-3} m/s). (a) Apparent relative velocity, V_r ; (b) Drag force coefficient, C_D .

Under various local parameters including mean diameter, relative velocity, drag force coefficient, volume fractions and physical properties of two phases, the local drag force can be quantified with Eqs. 4-10, and the results are shown in Fig. 12. It can be seen that drag force is higher at the gap between the plate and wall, which is in agreement with the previous work[46]. As the drag force is interaction force, the local drag force term is significant influenced by the profile of two-phase volume fraction.

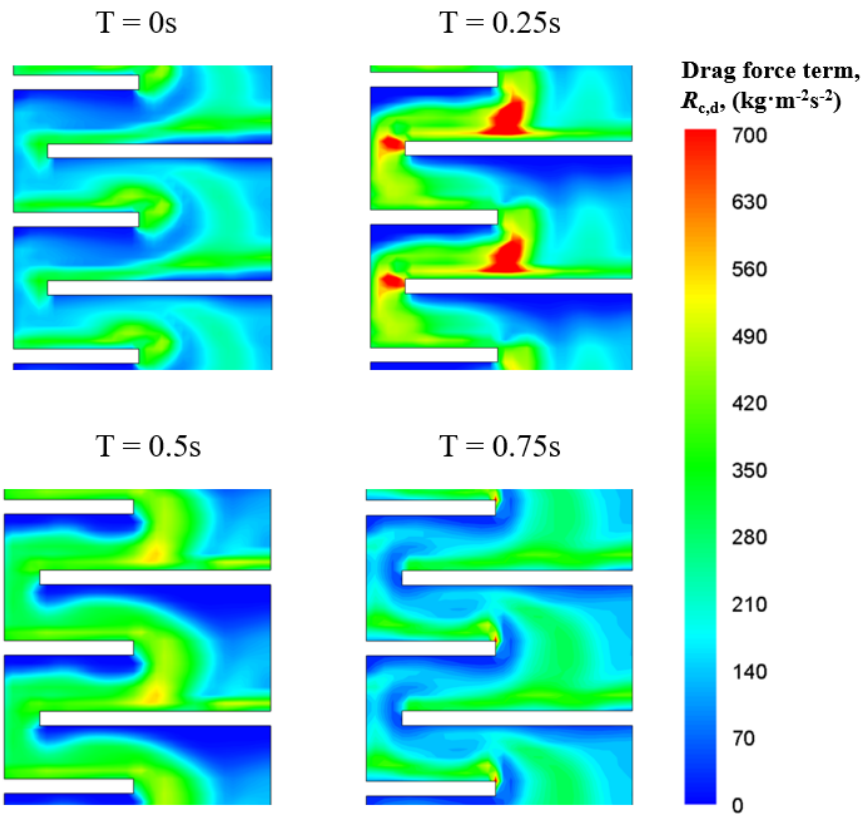

Fig. 12 Profile of drag force term during a pulsing period (Af =0.0153 m/s, V_c=6.25×10^{-4} m/s, V_d = 2.5×10^{-3} m/s)

Conclusion

In this work, the U-shape trend of dispersed holdup in pulsed disc and doughnut solvent extraction column have been simulated using a 2D two-fluid CFD approach. The following conclusions can be drawn from this study:

(i) Different drag models reported in literature are compared and the results show that CFD model could not accurately capture the increase of dispersed phase holdup. This can be attributed to the decrease of relative velocity, leading to underestimate drag force for high pulsation intensity.

(ii) A modified drag law is adopted by introducing turbulent viscosity and empirical constant, C , to account for the effect of the turbulence in increasing drag force coefficient. The value of $C$is also calculated based on Schiller and Nauman model and 0.5 is found more suitable to predict the U-shape trend of holdup of PDDC within 8.97% AARD.

(iii) The modified drag model is successfully implemented in the two-phase CFD-PBM simulations for U-shape trend of dispersed holdup predicting within 7.11% AARD.

(iv) Droplet size distribution predicted by the CFD-PBM simulation combined with the modified drag law is observed to be more precise than that of Schiller and Nauman drag law. The AARD ofd_{32} is 9.8% for the Schiller and Nauman drag law and 6.3% for the modified drag law.

(v) The local hydraulic performance and drag force field are illustrated to depict the flow characteristics of PDDC. These detailed results indicate the effects of operation and geometry parameters on the hydraulic

performance.

Acknowledgment

This work was financially supported by the Innovation Academy for Green Manufacture, Chinese Academy of Sciences (IAGM 2020DA02 and IAGM-2019-A15)

Nomenclature

A	stroke (twice the wave amplitude), m
$a\left(d,\ d^{'}\right)$	number coalescence rate of drops of diameter d with drops of diameter d', s^{-1}
$B^{B}\left(d,t\right)$	birth rate of droplets due to droplet breakup, $m^{-4}s^{-1}$
$B^{C}\left(d,t\right)$	birth rate of droplets due to droplet-droplet coalescence, $m^{-4}s^{-1}$
$\beta\left(d,d^{'}\right)$	daughter droplet size distribution function, dimensionless
$D^{B}\left(d,\ t\right)$	death rate of droplets due to droplet breakup, $m^{-4}s^{-1}$
$D^{C}\left(d,\ t\right)$	death rate of droplets due to droplet-droplet coalescence, $m^{-4}s^{-1}$
C_D	Drag force coefficient, dimensionless
d_{i}	drop diameter, m
d_{32}	Sauter mean drop diameter, m
d_c	column diameter, m
e	fractional free cross-sectional area, dimensionless
f	frequency, Hz
g	acceleration due to gravity, m/s^2
$\mathrm{g}\left(d\right)$	breakage frequency function, s^{-1}
$h\left(d,d^{'}\right)$	collision frequency function, s^{-1}
hc	compartment height, m
$n\left(d;\ x,\ t\right)$	number density function of the droplets, m^{-4}
Re	Reynolds number, dimensionless
$R_{c,d}$	Drag force term, kg $m^{-2}s^{-2}$
$V\ V_r$	superficial velocity, m/s relative velocity between two phases, m/s
v	volume, m^3
x_d	volume fraction holdup of the dispersed phase, dimensionless

Greek Symbols

γ	interfacial tension, N/m
ε	mechanical power dissipation per unit mass, m^2s^{-3}
$\lambda\left(d,d^{'}\right)$	coalescence efficiency function, dimensionless
$\mu\mu_{t,m}$	dynamic viscosity, Pa·s turbulent viscosity, Pa·s
ρ	density, kg/m^3

Subscripts

c	continuous phase
$D\ m$	dispersed phase mixture of the two phases

References

1. Marinsky JA, Marcus Y. *Ion Exchange and Solvent Extraction A Series of Advances.* Boca Raton, FL: CRC Press; 1995.**2.** Wang Y, Smith KH, Mumford KA, Yi H, Wang L, Stevens GW. Prediction of drop size in a pulsed and non-pulsed disc and doughnut solvent extraction column. *Chem. Eng. Res. Des.* 2016;109:667-674.**3.** Wang Y, Mumford KA, Smith KH, Li Z, Stevens GW. Dispersed-phase holdup and characteristic velocity in a pulsed and nonpulsed disk-and-doughnut solvent extraction column. *Ind. Eng. Chem. Res.* 2016;55(3):714-721.**4.** Torab-mostaedi M, Jalilvand H, Outokesh M. Dispersed phase holdup in a pulsed disc and doughnut extraction column. *Braz. J. Chem. Eng.* 2011;28(2):313-323.**5.** Liu J, Li S, Jing S. Hydraulic Performance of an Annular Pulsed Disc-and-Doughnut Column. *Solvent Extr. Ion Exch.*2015;33(4):385-406.**6.** Yadav RL, Patwardhan AW. Design aspects of pulsed sieve plate columns. *Chem. Eng. J.* 2008;138(1-3):389-415.**7.** Sarkar S, Sen N, Singh KK, Mukhopadhyay S, Shenoy KT. Effect of operating and geometric parameters on dispersed phase holdup in pulsed disc and doughnut and pulsed sieve plate columns: A comparative study. *Chem. Eng. Process.* 2017;118:131-142.**8.** Li W, Wang Y, Mumford KA, Smith KH, Stevens GW. Prediction of holdup and drop size distribution in a disc-doughnut pulsed column with tenova kinetics internals for the water-Alamine 336 system.*Hydrometallurgy.* 2018;181:82-90.**9.** Wang Y, Yi H, Smith KH, Mumford KA, Stevens GW. Mass transfer in a pulsed and non-pulsed disc and doughnut (PDD) solvent extraction column. *Chem. Eng. Sci.* 2017;165:48-54.**10.** Safari A, Safdari J, Abolghasemi H, Forughi M, Moghaddam M. Axial mixing and mass transfer investigation in a pulsed packed liquid-liquid extraction column using plug flow and axial dispersion models. *Chem. Eng. Res. Des.* 2012;90(2):193-200.**11.** Drumm C, Bart HJ. Hydrodynamics in a RDC extractor: Single and two-phase PIV measurements and CFD simulations. *Chem. Eng. Technol.* 2006;29(11):1297-1302.**12.** Hlawitschka MW, Jaradat M, Chen F, Attarakih MM, Kuhnert J, Bart H-J. A CFD-population balance model for the simulation of kühni extraction column. *Compt. Aided Chem. Eng.* 2011;29:66-70.**13.** Jaradat M, Attarakih M, Bart H-J. Population balance modeling of pulsed (packed and sieve-plate) extraction columns: coupled hydrodynamic and mass transfer. *Ind. Eng. Chem. Res.*2011;50(24):14121-14135.**14.** Retieb S, Guiraud P, Angelov G, Gourdon C. Hold-up within two-phase countercurrent pulsed columns via Eulerian simulations.*Chem. Eng. Sci.* 2007;62(17):4558-4572.**15.** Yadav RL, Patwardhan AW. CFD modeling of sieve and pulsed-sieve plate extraction columns. *Chem. Eng. Res. Des.*2009;87(1):25-35.**16.** Yi H, Wang Y, Smith KH, Fei W, Stevens GW. CFD simulation of liquid-liquid two-phase hydrodynamics and axial dispersion analysis for a non-pulsed disc and doughnut solvent extraction column.*Solvent Extr. Ion Exch.* 2016;34(6):535-548.**17.** Yu X, Zhou H, Jing S, Lan W, Li S. 3D-CFD simulation of liquid-liquid two-phase flow in a pilot-plant scale annular pulsed disc and doughnut column. *Solvent Extr. Ion Exch.* 2018;36(5):480-498.**18.** Yi H, Smith KH, Fei W, Stevens GW. CFD Simulation of Two-Phase Flow in a Hybrid Pulsed Sieve-Plate Solvent Extraction Column: Prediction of Holdup and Axial-dispersion Coefficients. *Solvent Extr. Ion Exch.* 2019;38(1):88-102.**19.** Saini RK, Bose M. Stage holdup of dispersed phase in disc and doughnut pulsed column. *Energ. Procedia.* 2014;54:796-803.**20.** Sarkar S, Singh KK, Shenoy KT. Two-phase CFD modeling of pulsed disc and doughnut column: Prediction of dispersed phase holdup.*Sep. Purif. Technol.* 2019;209:608-622.**21.** Sarkar S, Singh KK, Shenoy KT. CFD modeling of pulsed disc and doughnut column: prediction of axial dispersion in pulsatile liquid-liquid two-phase flow. *Ind. Eng. Chem. Res.*2019;58(33):15307-15320.**22.** Wallis GB. *One-dimensional two-phase flow.* New York: McGraw-Hill Book Company; 1969.**23.** Sen N, Singh K, Patwardhan A, Mukhopadhyay S, Shenoy K. CFD simulation of two-phase flow in pulsed sieve-plate column – Identification of a suitable drag model to predict dispersed phase hold up. *Sep. Sci. Technol.* 2016;51(17):2790-2803.**24.** Kumar A, Hartland S. Gravity settling in liquid/liquid dispersions. *Can. J. Chem. Eng.* 1985;63(3):368-376.**25.** Coulaloglou CA, Tavlarides LL. Description of interaction processes in agitated liquid-liquid dispersions. *Chem. Eng. Sci.*1977;32(11):1289-1297.**26.** Amokrane A, Charton S, Sheibat-Othman N, Becker J, Klein JP, Puel F. Development of a CFD-PBE coupled model for the simulation of the drops behaviour in a pulsed column. *Can. J. Chem. Eng.*2014;92(2):220-233.**27.** Amokrane A, Maaß S, Lamadie F, Puel F, Charton S. On droplets size distribution in a pulsed column. Part I: In-situ measurements and corresponding CFD–PBE simulations. *Chem. Eng. J.* 2016;296:366-376.**28.** Zhou H, Jing S, Fang Q, Li S, Lan W. Direct measurement of droplet breakage in a pulsed disc and doughnut column. *AlChE J.*2017;63(9):4188-4200.**29.** Yu X, Zhou H, Jing S, Lan W, Li S. CFD–PBM simulation of two-phase flow in a pulsed disc and doughnut co-

lumn with directly measured breakup kernel functions. *Chem. Eng. Sci.*2019;201:349-361.**30.** Sen N, Singh KK, Patwardhan AW, Mukhopadhyay S, Shenoy KT. CFD-PBM simulations of a pulsed sieve plate column. *Prog. Nucl. Energ.* 2019;111:125-137.**31.** Zhang JW, Y.;Stevens, G.W.;Fei, W. An experimental study on single drop rising in a low interfacial tension liquid–liquid system.*Chem. Eng. Res. Des.* 2019;148:349-360.**32.** Augier F, Masbernat O, Guiraud P. Slip velocity and drag law in a liquid-liquid homogeneous dispersed flow. *AlChE J.*2003;49(9):2300-2316.**33.** Jildeh HB, Attarakih M, Bart H-J. Droplet coalescence model optimization using a detailed population balance model for RDC extraction column. *Chem. Eng. Res. Des.* 2013;91(7):1317-1326.**34.** Tavlarides MAHaLL. Simulation analysis of drop breakage, coalescence and micromixing in liquid-liquid stirred tanks. *Chem. Eng. J.* 1983;26(3):189-199.**35.** Drumm C, Attarakih M, Hlawitschka MW, Bart H-J. One-Group Reduced Population Balance Model for CFD Simulation of a Pilot-Plant Extraction Column. *Ind. Eng. Chem. Res.* 2010;49(7):3442-3451.**36.** Din GU, Chughtai IR, Inayat MH, Khan IH, Qazi NK. Modeling of a two-phase countercurrent pulsed sieve plate extraction column—A hybrid CFD and radiotracer RTD analysis approach. *Sep. Purif. Technol.* 2010;73(2):302-309.**37.** Schiller L, Naumann Z. *Verein Deutshen Ingenieure Zeitung*1935.**38.** Bardin-Monnier N, Guiraud P, Gourdon C. Residence time distribution of droplets within discs and doughnuts pulsed extraction columns via Lagrangian experiments and simulations. *Chem. Eng. J.*2003;94(3):241-254.**39.** Wen CY, Yu YH. Mechanics of fluidization. *American Institution of Chemical Engineers Symposium Series.* 1966;62:100-111.**40.** Ishii M, Zuber N. Drag coefficient and relative velocity in bubbly, droplet or particulate flows. *AlChE J.*1979;25(5):843-855.**41.** Onink F, Drumm C, Meindersma GW, Bart H-J, de Haan AB. Hydrodynamic behavior analysis of a rotating disc contactor for aromatics extraction with 4-methyl-butyl-pyridinium·BF4 by CFD.*Chem. Eng. J.* 2010;160(2):511-521.**42.** Kerdouss F, Bannari A, Proulx P. CFD modeling of gas dispersion and bubble size in a double turbine stirred tank. *Chem. Eng. Sci.* 2006;61(10):3313-3322.**43.** Amokrane A, Charton S, Lamadie F, Paisant JF, Puel F. Single-phase flow in a pulsed column: Particle image velocimetry validation of a CFD based model. *Chem. Eng. Sci.* 2014;114:40-50.**44.** Li W, Wang Y, Mumford KA, Smith KH, Stevens GW. Comparison of the hydrodynamic performance of pulsed solvent extraction columns with tenova pulsed column kinetics internals and standard disc and doughnut internals for copper extraction using the LIX 84 system.*Solvent Extr. Ion Exch.* 2017;35(5):303-320.**45.** Kumar A, Hartland S. Prediction of dispersed phase hold-up in pulsed perforated-plate extraction columns. *Chem. Eng. Process.* 1988;23(1):41-59.**46.** McAllister RA, Groenier WS, Ryon AD. Correlation of flooding in pulsed, perforated-plate extraction columns. *Chem. Eng. Sci.* 1967;22(7):931-944.**47.** Kerdouss F, Bannari A, Proulx P, Bannari R, Skrga M, Labrecque Y. Two-phase mass transfer coefficient prediction in stirred vessel with a CFD model. *Computers & Chemical Engineering.*2008;32(8):1943-1955.**48.** A. B, H.E.A. VdA. A Computational Model for the Gas-Liquid Flow in Stirred Reactors. *Chemical Engineering Research and Design.* 1994;72(4):573-582.**49.** Mednick EBL. A generalised approach to the fluid dynamics of particulate systems part 2: Sedimentation and fluidisation of clouds of spherical liquid drops. *Can. J. Chem. Eng.* 1975;53(5):461-468.**50.** Tan B, Lan M, Li L, Wang Y, Qi T. Drop size correlation and population balance model for an agitated-pulsed solvent extraction column. *AIChE J.* 2020;e16279.